Supporting Information

Unravel the Catalytic Effect of 2-Dimmensional Metal Sulfides on Polysulfides Conversions for Lithium-Sulfur Batteries

Chunli Wang[1,2], Lianshan Sun[3], Kai Li [1,], Zhijian Wu[1], Feifei Zhang[4,]*, Limin Wang [1,]**

[1]State Key Laboratory of Rare Earth Resource Utilization, Changchun Institute of Applied Chemistry, Chinese Academy of Sciences, Changchun, 130022, P. R. China

[2]School of Applied Chemistry and Engineering, University of Science and Technology of China, Hefei, 230026, P. R. China

[3]Institute for Energy Research, Key Laboratory of Zhenjiang, Jiangsu University, Zhenjiang 212013, PR China

[4]Department of Materials Science and Engineering, Faculty of Engineering, National University of Singapore, 117576, Singapore

E-mail: kaili@ciac.ac.cn, msezf@nus.edu.sg, lmwang@ciac.ac.cn

Experimental Section

1. Materials Preparations

In a typical synthesis, 100 mg of Na_2CrO_4, $(NH_4)_7Mo_6O_{24}$, Na_2WO_4 was dissolved into 5 mL of deionized water, respectively; then 100 mg dopamine hydrochloride was added into the above solution to form Cr-DA, Mo-DA and W-DA complexes. Each of the resulting solution was added into 40 g of NaCl and 2 g of thiourea and stirred uniformly until the solution is fully absorbed by the template nanoparticles. The solid particles were freeze-dried at −45 °C to remove water in the mixture. After annealing the prepared precursors at 700 ^oC for 5 h under Ar/H_2 atmosphere, the products were obtained after removing NaCl by filtering with water several times and dried at 60 °C for 12 h. Similarly, the carbon matrix was synthesized through the same method without the addition of metalate salts. Synthesis of the NCs-S, Cr_3S_4/C-S, MoS_2/C-S and WS_2/C-S was performed by mixing sulfur powder with the as-prepared products, then sealing in a Teflon-lined stainless-steel autoclave (N_2 atmosphere), and heating at 155 ^oC for 12 h and 200 ^oC for 2 h.

2. Material characterizations:

SEM characterizations were conducted on Hitachi S-4800 field emission scanning electron microscopy. Transmission electron microscopy (TEM), high-resolution TEM (HRTEM) images and energy-dispersive X-ray spectroscopy (EDX) element mapping were performed using a FEI Tecnai G2 S-Twin instrument. X-ray diffraction (XRD) patterns were determined by a Bruker D8 Focus power X-ray diffractometer using Cu Kα radiation. A STA 449 °C Jupiter (NETZSCH) thermogravimetry instrument was used for Thermogravimetric (TGA) analysis. The N_2 adsorption–desorption isotherm was performed on a Micromeritics ASAP 2020 instrument. X-ray photoelectron spectroscopy (XPS) characterizations were carried out in an ESCALAB 250 instrument with 150W Al Kα probe beam. The surface area measurement was performed on Micromeritics ASAP 2010 instrument. Raman spectra characterizations were performed on a T64000 instrument from JY company from French.

3. Preparation of Lithium Polysulfides (Li_2S_6)

Li_2S_6 solution was prepared first by mixing Li_2S and sulfur at a molar ratio of 1:5 in a solution with 1 M lithium bis (trifluoromethane sulfonyl) imide (LiTFSI) in 1,3-dioxolane (DOL) and 1,2-dimethoxyethane (DME) (v/v 1:1), followed by stirring at 60 ^oC for two days inside an argon-filled glove box.

4. Visualized Adsorption and catalytic studies of LiPSs

Typically, NCs, Cr_3S_4/C, MoS_2/C and WS_2/C with surface areas of 1 m^2 were dispersed individually into the solutions with 5 mL Li_2S_6 concentration of 12.5 mmol L^{-1}, respectively. After standing for 5 h, via observing the color change in the supernatant of residual LiPSs, the level of the adsorption ability for LiPSs of the above products was initially determined. Finally, the precipitates denoted as Cr_3S_4–Li_2S_6, MoS_2–Li_2S_6 and WS_2–Li_2S_6 were obtained by centrifugation to analyze the states of the material surface by XPS tests.

5. Assembly of symmetric cells and kinetic evaluation of polysulfide conversion

The corresponding electrodes were fabricated with NCs, Cr_3S_4/C, MoS_2/C and WS_2/C composites, where the active material and poly(vinylidene fluoride) (PVDF) with the mass ratio of 5:1 were dispersed in N-methyl pyrrolidone (NMP) solution to form uniform slurry and then chopped into the round electrode piece of 12 mm with ~2 mg mass loading. The symmetrical 2025 coin cells (Li_2S_6-Li_2S_6) with a Celgard 2400 membrane as separator were fabricated and those disks were used as identical working and counter electrodes containing 40 μL electrolyte of 0.2 M Li_2S_6. Same electrolyte without Li_2S_6 was used as a control. The cyclic voltammetry (CV) and electrochemical impedance spectroscopy (EIS) measurements of the symmetrical cells were operated at a scan rate of 1 and 100 mV s^{-1} with the voltage window between from -1 V to 1 V.

The electrocatalytic activity of NCs, Cr_3S_4/C, MoS_2/C and WS_2/C toward LiPSs conversion reactions were further measured by nucleation of Li_2S on different reactive surfaces using CV. The asymmetrical 2025 coin cells were probed, where a piece of lithium foil worked as the

counter electrode, an identical new electrode used in aforementioned kinetic study served as the working electrode, 20 μL of 0.2 M Li_2S_6 solution (0.768 mg based on S) was applied as catholyte, and 20 μL of control electrolyte without Li_2S_6 was used as anolyte. The assembled cells were firstly galvanostatically discharged at 0.15 mA to 1.80 V for full transformation of LiPSs species into solid Li_2S on catalytically reactive interfaces then potentiostatically charged at 2.40 V for the oxidization of Li_2S into soluble LiPSs using a programmable battery testing system (LAND CT2001A). Reversely, the assembled cells were discharged galvanostatically at 0.15 mA to 2.08 V and then discharged potentiostatically at 2.07 V for Li_2S nucleation and growth on a Bio-Logic VMP3 Electrochemical Workstation. The potentiostatic discharge was terminated the charge current was below 10^{-5} A.

6. Electrochemical measurements:

The electrodes were made by mixing 70% sulfur-impregnated powders, 20% carbon black and 10 % polyvinylidene fluoride (PVDF) with 1-methyl-2-pyrrolidinone (NMP), then coated evenly onto carbon-coated aluminum foil. This film was then dried at 40 °C in a vacuum oven for 12 h, and cut into discs with a typical diameter of 12 mm, where the content of active material was around ~1.4 mg. A solution of 1 M (LITFSI) and 0.1 M lithium nitrate ($LiNO_3$) dissolved in mixed solvent of dimethoxyethane (DME) and 1, 3-dioxolane (DOL) with a volume ratio of 1:1 was employed as electrolyte. The coin cells (CR-2025) were assembled glove box where 30 μL of the electrolyte was added to wet the sulfur cathode, a Celgard 2400 separator was then placed over the electrode, and the lithium foil anode with a size of 14 mm was placed on top of the separator. The discharge/charge performances were tested galvanostatically using a programmable battery testing system (LAND CT2001A) at room temperature under different C-rates (1 C = 1675 mA g^{-1}) within a potential range of 1.7–2.6 V. CV measurements were conducted with a scanning rate of 0.1 mV s^{-1} and the potential *vs.* Li^+/Li ranging from 1.7 to 2.8 V on a Bio-Logic VMP3 Electrochemical Workstation.

7. Computational Details

The calculations were carried out using density functional theory (DFT+U) with the Perdew-Burke-Ernzerbof (PBE) form of generalized gradient approximation functional (GGA). [1] The Vienna ab-initio simulation package (VASP) [2-4] was employed. The plane wave energy cutoff was set as 400 eV. The Fermi scheme was employed for electron occupancy with an energy smearing of 0.1 eV. The first Brillouin zone was sampled in the Monkhorst−Pack grid [5]. The 3×3×1 k-point mesh for the calculations. The energy (converged to 1.0 $\times 10^{-6}$ eV/atom) and force (converged to 0.01eV/Å) were set as the convergence criterion for geometry optimization. The spin polarization was considered in all calculation.

Models

The Cr_3S_4 (-202), MoS_2 (100) and WS_2 (100) surfaces show high intensities in XRD, thus the targeted simulative structures were selected by cutting the corresponding bulk along [-202], [100] and [100] crystal planes, separately. A vacuum layer as large as 15 Å was used along the direction normal to the surface to avoid periodic interactions. The equations of the lithiation process could be presented as follows:

$S_8 + 2e^- + 2Li^+ \rightarrow Li_2S_8$

$3Li_2S_8 + 2e^- + 2Li^+ \rightarrow 4Li_2S_6$

$2Li_2S_6 + 2e^- + 2Li^+ \rightarrow 3Li_2S_4$

$Li_2S_4 + 2e^- + 2Li^+ \rightarrow 2Li_2S_2$

$Li_2S_2 + 2e^- + 2Li^+ \rightarrow 2Li_2S$

And the Gibbs free energy changes (ΔG) of the corresponding reactions on catalytically reactive interfaces have been investigated. The ΔG is defined as follows [6] :

$$\Delta G_1 = G_{Li_2S_8} - \left(G_{S_8} + 2\mu_{Li}\right)$$

$$\Delta G_2 = G_{Li_2S_6} - \left(3/4G_{Li_2S_8} + 2/4\mu_{Li}\right)$$

$$\Delta G_3 = G_{Li_2S_4} - \left(2/3G_{Li_2S_6} + 2/3\mu_{Li}\right)$$

$$\Delta G_4 = G_{Li_2S_2} - \left(1/2G_{Li_2S_4} + \mu_{Li}\right)$$

$$\Delta G_5 = G_{Li_2S} - \left(1/2G_{Li_2S_2} + \mu_{Li}\right)$$

where G_{S_8}, $G_{Li_2S_8}$, $G_{Li_2S_6}$, $G_{Li_2S_4}$, $G_{Li_2S_2}$, and G_{Li_2S} is the total energy of these polysulfides adsorbed on Cr_3S_4, MoS_2 and WS_2 surfaces, respectively. And μ_{Li} is the chemical potential of the Li.

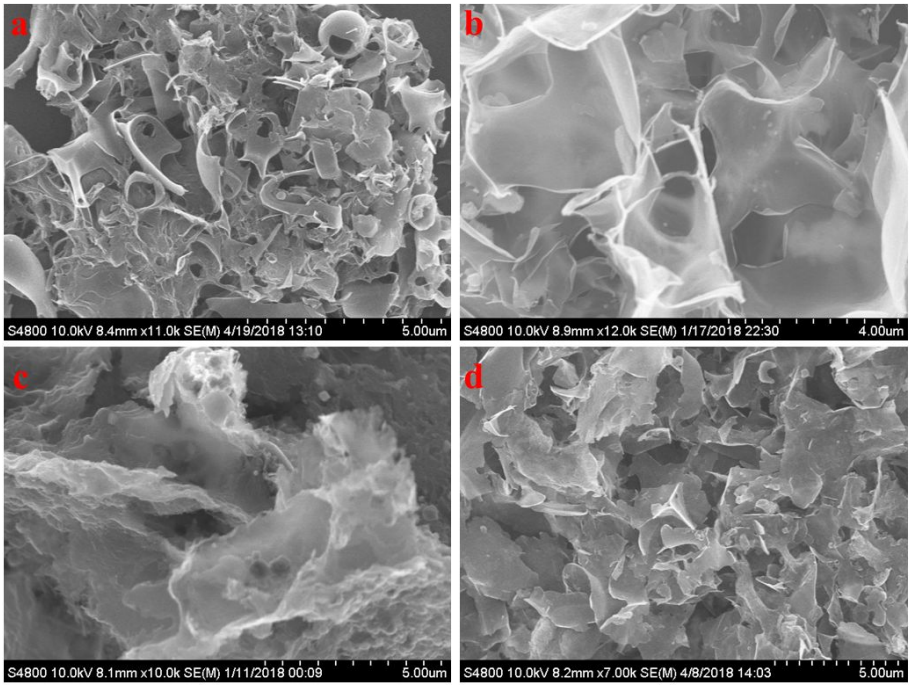

Figure S1. SEM images of (a) NCs, (b) Cr_3S_4/C, (c) MoS_2/C and (d) WS_2/C flakes.

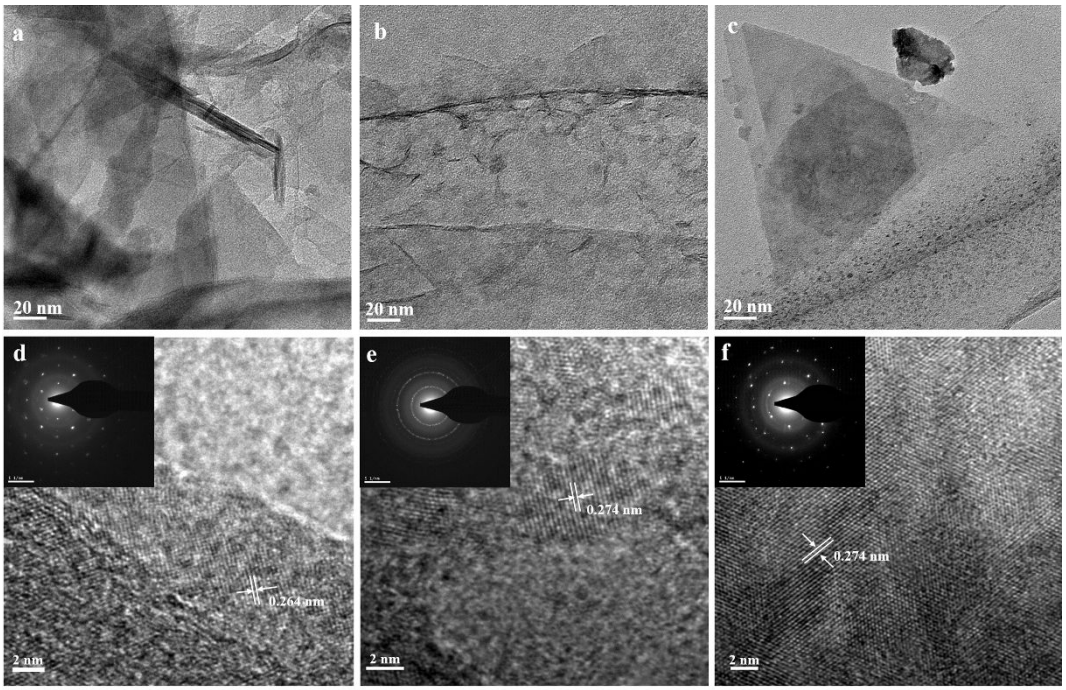

Figure S2. Typical TEM images and HRTEM image of (a, d) Cr_3S_4/C, (b, e) MoS_2/C and (c, f)WS_2/C flakes; the insets are the corresponding SAED patterns.

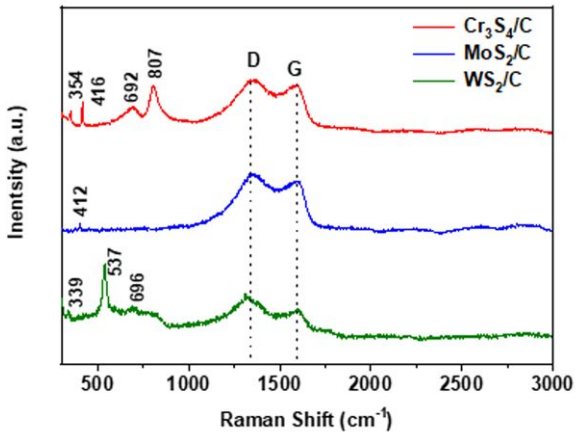

Figure S3. Raman spectrums of Cr_3S_4/C, MoS_2/C and WS_2/C flakes.

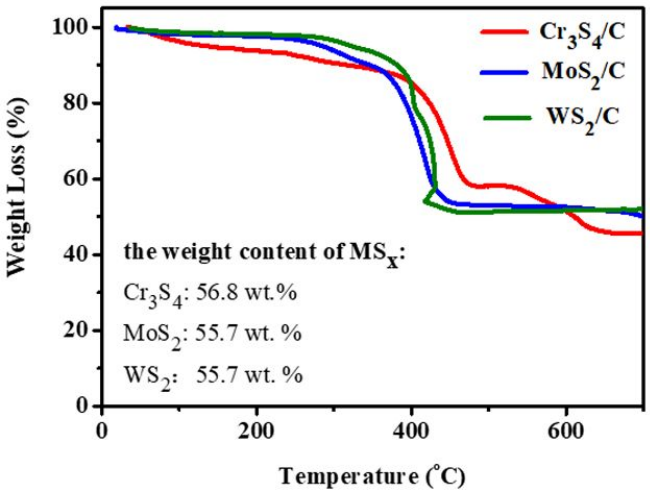

Figure S4. TGA curves of Cr_3S_4/C, MoS_2/C and WS_2/C flakes under air atmosphere.

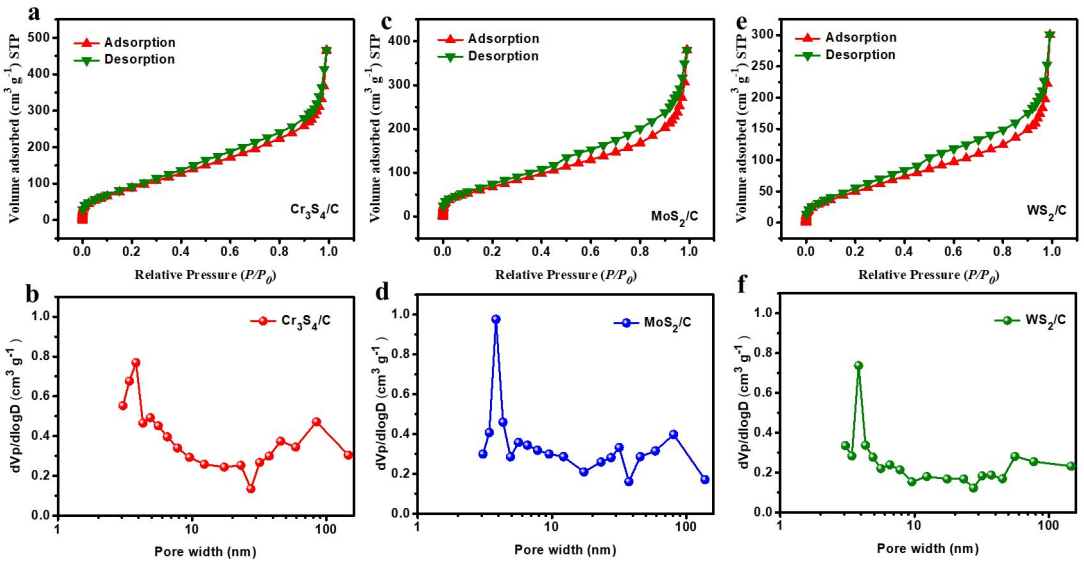

Figure S5. N_2 adsorption–desorption isotherms of (a) Cr_3S_4/C, (c) MoS_2/C, (e) WS_2/C and pore size distribution of (b) Cr_3S_4/C, (d) MoS_2/C, (f) WS_2/C.

Table S1. Physical properties of Cr_3S_4/C, MoS_2/C and WS_2/C.

samples	BET ($m^2\ g^{-1}$)	Pore Volume ($cm^3\ g^{-1}$)	Micro Pore Volume ($cm^3\ g^{-1}$)	PSD (nm)
Cr_3S_4/C	354.8	0.72	0.12	8.11
MoS_2/C	259.5	0.59	0.094	9.07
WS_2/C	196.8	0.47	0.068	9.44

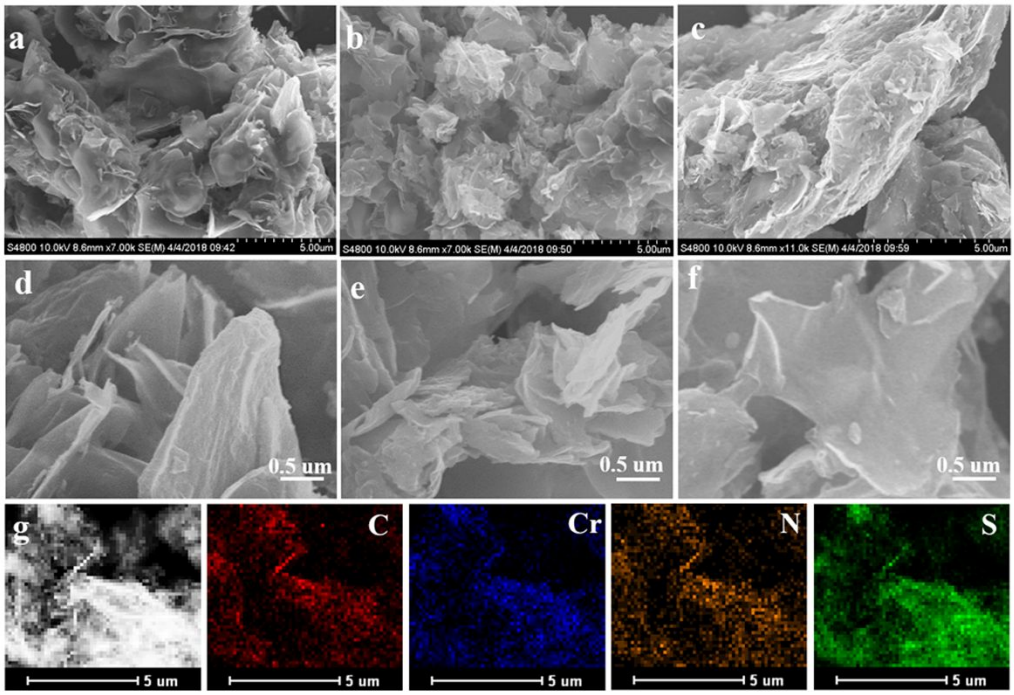

Figure S6. the SEM images of (a, d) Cr_3S_4/C-S, (b, e) MoS_2/C-S, (c, f) WS_2/C-S; (g) the EDX mappings of Cr_3S_4/C-S with C, Cr, S elements.

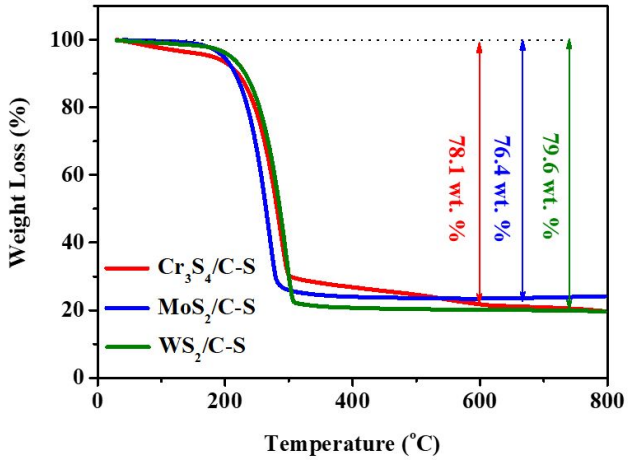

Figure S7. The TGA curves of Cr_3S_4/C-S, MoS_2/C-S and WS_2/C-S.

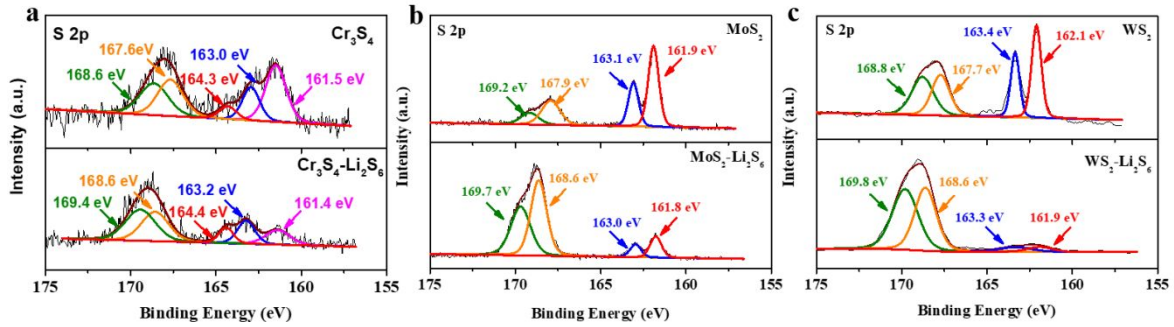

Figure S8. the high resolution XPS spectrums of S 2p of (a) Cr_3S_4/C, (b) MoS_2/C, (c) WS_2/C before and after Li_2S_6 adsorption.

Table S2. The peaks of the symmetric cells of NCs, Cr_3S_4/C, MoS_2/C and WS_2/C.

Samples / Peaks (V)	NCs	Cr_3S_4/C	MoS_2/C	WS_2/C
Peak Ⅰ	0.194	0.108	0.153	0.08
Peak Ⅱ	0.53	0.358	0.409	0.305
Peak Ⅲ	-0.207	-0.103	-0.142	-0.112
Peak Ⅳ	-0.518	-0.387	-0.387	-0.454

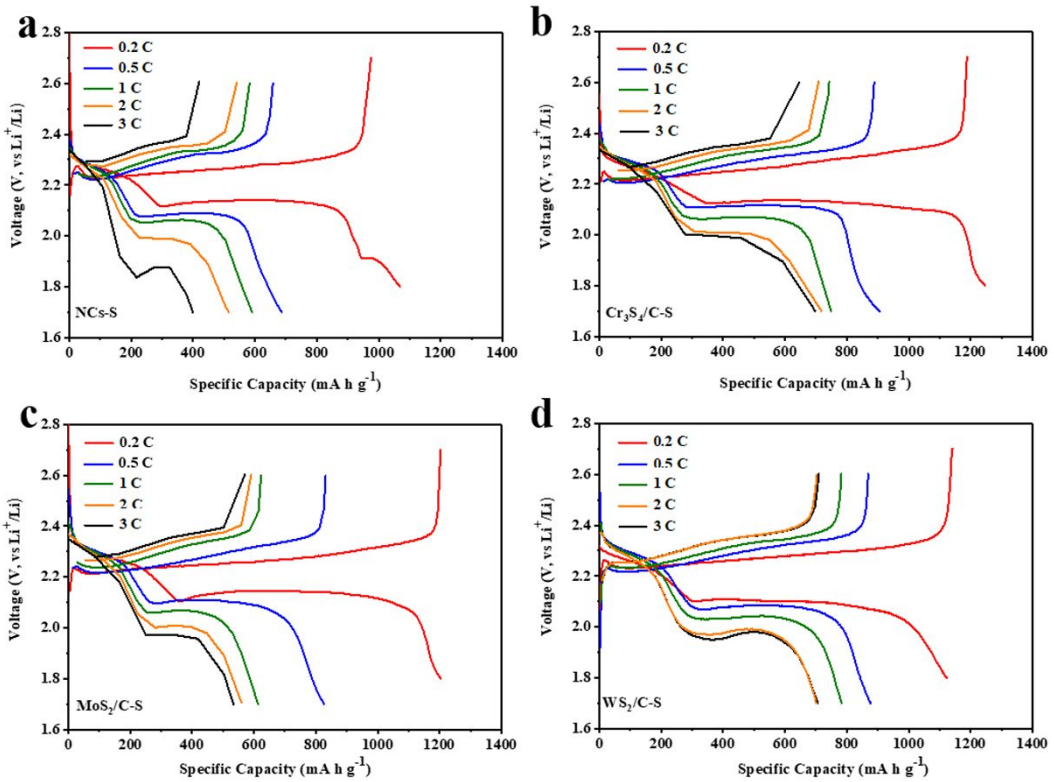

Figure S9. The discharge/charge curves at different current densities for (a) NCs-S, (b)Cr_3S_4/C-S, (c) MoS_2/C-S and (d) WS_2/C-S electrodes.

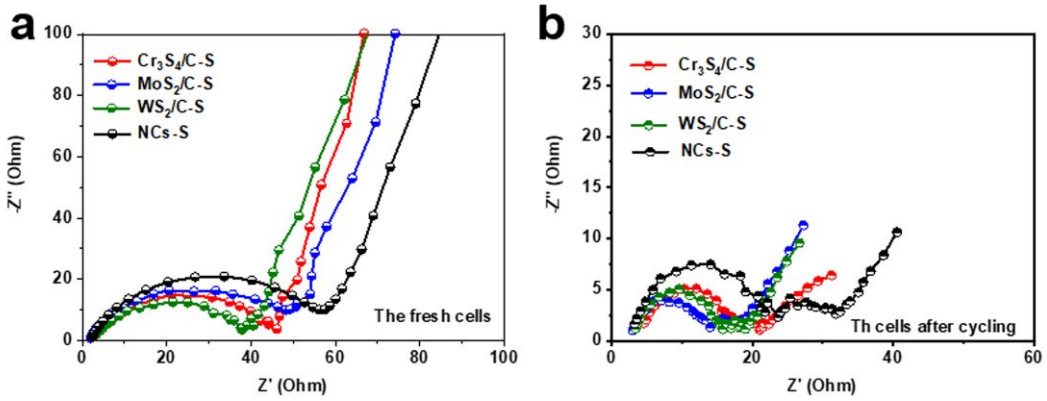

Figure S10. The EIS spectrums of (a) the fresh cells and (b) the cells after cycling 150 th cycles at 0.2 C based of the composites.

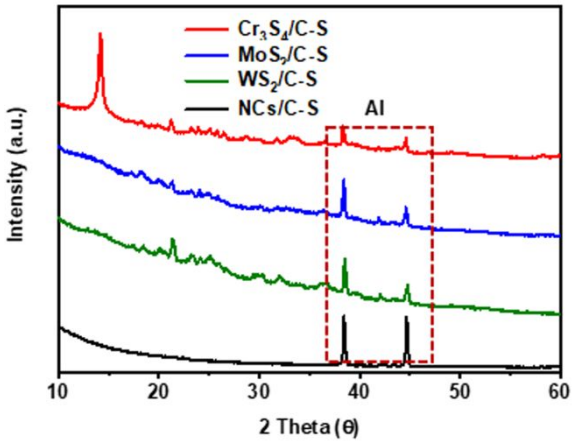

Figure S11. The XRD patterns of the cathodes after cycling 100 th cycles.

Table S3. Electrochemical performances of LSBs based on various metal sulfides materials

Host materials	S content (wt. %)	The active material loading (mg cm^{-2})	Specific surface area (mg cm^{-3})		Cycle capacity (mA h g^{-1})		Ref.
			Catalyst content (%)		Initial	Retention	
Cr_3S_4/C	78.1	0.8-1	354.8	12.4	1288	840 (150 cycles at 0.2 C)	***This work***
Pt/graphene	N/A	N/A	N/A	N/A	1108	780 (100 cycles at 0.2 C)	9
NiS_2/C	54.9	0.8–1.3	N/A	N/A	1153	730 (200 cycles at 0.5 C)	16
WS_2-WS_2/CCI	N/A	~3	N/A	N/A	1500	1000 (500 cycles at 0.5 C)	17
MoS_{2-x}/rGO	75	2-4	N/A	12	1160	820 (150 cycles at 0.5 C)	18
CoS_2/Graphene	75	0.4	709	15	1368	1005 (150 cycles at 0.5 C)	30
WS_2/Graphene	70	2.7	N/A	4	931.7	696.2 (500 cycles at 1 C)	58

Tables S4. The Gibbs free energy of Li_2S_x during lithiation on Cr_3S_4, MoS_2 and WS_2.

Samples / Gibbs free energy (eV)	Cr_3S_4	MoS_2	WS_2
ΔG_1	-3.64	-2.73	-3.84
ΔG_2	-2.25	-1.95	-3.17
ΔG_3	-4.67	-4.54	-2.2
ΔG_4	-7.55	-6.4	-8.52
ΔG_5	-9.2	-5.85	-11.7

Reference

[1] J P Perdew, K Burke, M Ernzerhof, *Phys. Rev. Lett.* **1996**, 77, 3865.

[2] G Kresse, J Hafner, *Phys. Rev. B.* **1993**, 47**,** 558.

[3] G Kresse, J Hafner, *Phys. Re. B* **1994**, 49, 14251.

[4] G Kresse, J Furthmüller, Phys. Rev. B **1996**, 54, 11169.

[5] H J Monkhorst, J D Pack, *Phys. Rev. B* **1976**, 13, 5188.

[6] J Wu, L W Wang. *J. Mater. Chem. A.* **2018**, 6**,** 2984.